



Synthesis of high surface area TiO₂ nanoparticles by mild acid treatment with HCl or HI for photocatalytic propene oxidation

M. Ouzzine^a, J.A. Maciá-Agulló^b, M.A. Lillo-Ródenas^{a,*}, C. Quijada^c, A. Linares-Solano^a

^a Grupo de Materiales Carbonosos y Medioambiente, Dpto. Química Inorgánica, Facultad de Ciencias, Universidad de Alicante, Ap. 99, E-03080 Alicante, Spain

^b Instituto Nacional del Carbón (CSIC), Apartado 73, 33080 Oviedo, Spain

^c Depto. de Ingeniería Textil y Papelera, Universitat Politècnica de València, Plaza de Ferrándiz y Carbonell s/n, 03801 Alcoy (Alicante), Spain

ARTICLE INFO

Article history:

Received 18 December 2013

Received in revised form 14 February 2014

Accepted 19 February 2014

Available online 28 February 2014

Keywords:

TiO₂ nanoparticles

Acid-ethanol

Low temperature

Photocatalytic activity

Propene

ABSTRACT

Nanostructured TiO₂ photocatalysts with small crystalline sizes have been synthesized by sol-gel using the amphiphilic triblock copolymer Pluronic P123 as template. A new synthesis route, based on the treatment of TiO₂ xerogels with acid-ethanol mixtures in two different steps, synthesis and extraction-crystallization, has been investigated, analyzing two acids, hydrochloric and hydriodic acid. As reference, samples have also been prepared by extraction-crystallization in ethanol, being these TiO₂ materials amorphous and presenting higher porosities. The prepared materials present different degrees of crystallinity depending on the experimental conditions used. In general, these materials exhibit high surface areas, with an important contribution of microporosity and mesoporosity, and with very small size anatase crystals, ranging from 5 to 7 nm.

The activity of the obtained photocatalysts has been assessed in the oxidation of propene in gas phase at low concentration (100 ppmv) using a UVA lamp with a wavelength of 365 nm. Under the conditions studied, these photocatalysts show different activities in the oxidation of propene which do not depend on their surface areas, but on their crystallinity and band gap energies. Sample prepared with HCl both during synthesis and in extraction-crystallization steps is the most active one, with superior performance than Evonik P25.

© 2014 Elsevier B.V. All rights reserved.

1. Introduction

Heterogeneous photocatalytic oxidation (PCO) has been extensively investigated as a method to oxidize organic pollutants in water and air [1–3]. PCO is a promising technology to decompose at ambient temperature some volatile organic compounds (VOCs) of low concentration. Propene is considered a highly reactive volatile organic compound which is involved in the formation of ground-level and tropospheric ozone and, therefore, in photochemical smog [4,5]. Propene is one of the major sources of indoor air pollution as it is one of the principal components of tobacco smoke, together with other alkenes [6]. Titanium dioxide (TiO₂) has been successfully employed for the photocatalytic oxidation of propene at low concentration and room temperature [7–12]. TiO₂ is an interesting material as semiconductor, having high photochemical stability and being easily available and cheap [13]. However,

the preparation conditions under which the TiO₂ powders are synthesized lead to significant variation in their structure, particle size, specific surface area, crystallinity, pore structure, and hence, photoactivity [14,15].

The photocatalytic activity mainly depends on the material's crystallinity and specific surface area. A good crystallinity is often required to reduce the formation of electron traps, which might affect the photocatalytic efficiency [16], and a large specific surface area can supply more active sites and higher number of adsorbed substrates [17]. To obtain highly active TiO₂ photocatalysts, therefore, it is important to maximize simultaneously these two properties. However, the synthesis of stable titania with high crystallinity and large surface area is still a challenge.

The effect of particle size on the photoactivity of TiO₂ was investigated by several researchers [12,17–20]. Experimental research led to the discovery that, for a given application, an optimum particle size of TiO₂ exists such that the photocatalytic oxidation rates of organic substrates are maximized [15]. Titania nanoparticles with very fine sizes are promising in many applications [17,20,21]. In almost all of these cases, when the particle size is greatly reduced

* Corresponding author. Tel.: +34 965 909350; fax: +34 965 903454.
E-mail address: mlillo@ua.es (M.A. Lillo-Ródenas).

due to a large surface to volume ratio, especially to several nanometers' scale, some novel optical properties can be expected [22]. It is not surprising, therefore, that an intense research has been focused upon the reduction of particle size. It was usually found that different routes often produce different results [23–25]. So, it is interesting to continue investigating in detail the methods which may have an important effect on the particle size.

There are many low temperature methods available for the synthesis of small TiO_2 nanoparticles, such as ultrasonic irradiation [26], UV light assistance [27], solvent evaporation-induced crystallization [28], sol–gel [29] and so on. Among these methods, the sol–gel method is the most widely employed due to the inexpensive equipment required, the low temperatures used and the homogeneous and highly pure product produced. Usually, the crystallization of TiO_2 has been carried out by processes such as severe calcination and hydrothermal treatment [30,31]. The use of high temperatures would result in the growth of crystal particles, causing structural collapse and, therefore, decrease in the specific surface area of TiO_2 . A reasonable pathway to avoid these problems would be to lower the temperature of the phase transition [32] and, in this sense, methods based on crystallization of titania by mild acid treatments are being studied [33–35]. The novelty of this work is to study the influence of hydriodic acid (HI) in the synthesis and extraction–crystallization steps and hence on the properties of TiO_2 nanoparticles, and also the application of the prepared materials in the photocatalytic oxidation of propene, since the catalysts previously prepared were used for the removal of contaminants in liquid phase, showing low activity.

Additionally, it is also known that in the presence of a typical surfactant, micro/mesoporous structures might be generated via sol–gel route [36]. The micropores formation depends on the contribution of important factors such as: (i) the inclusion of the surfactant groups into the TiO_2 framework, (ii) the low condensation degree of titania derived from the acidic synthesis conditions and (iii) the subsequent treatment of the obtained xerogel with acid mixtures under reflux that provides micro/mesoporous TiO_2 , exhibiting remarkable textural properties based on anatase nanocrystallites [36].

Considering these aspects, in the present work we have synthesized TiO_2 nanoparticles using surfactant-assisted templating sol–gel method. The Pluronic P123 is used as non-ionic surfactant in order to obtain mesoporous titanium dioxide with small anatase crystal size. This preparation method is based on a two-step procedure: (i) the preparation of the amorphous TiO_2 and (ii) the control of the crystalline phase growth of the sample by acid–ethanol treatment. The first step takes place by sol–gel in acidic conditions, and leads to the formation of complexes between polarized carbonyl active groups of P123 and titanium cations [37], leading the hydrophilic/hydrophobic interactions to the formation of the mesostructure. The second step, that is referred to in the manuscript as extraction–crystallization, involves an acid–ethanol treatment, which leads to the removal of the Pluronic P123 surfactant and allows to improve the phase transition from amorphous phase to anatase, while the good textural properties previously produced are greatly preserved.

The effect of the nature of the acid used as catalyst in the xerogel synthesis process of the surfactant-assisted templating method (either HCl or HI) and the influence of the treatment used in the extraction–crystallization (with HCl–EtOH or HI–EtOH under reflux) on the physical properties of the nanocrystalline titania were thoroughly studied. Finally, the physical properties of the prepared titania samples were also studied in relation to their photocatalytic activity in the oxidation of propene in gas phase at low concentration (100 ppmv) at room temperature under UV-light sources with wavelength of 365 nm.

2. Experimental

2.1. Chemicals

Reagents used for the synthesis included an amphiphilic triblock copolymer (commercially referred to as Pluronic P123 polyethylene oxide–polypropylene oxide–polyethylene oxide ($\text{PEO}_{20}\text{PPO}_{70}\text{PEO}_{20}$), and titanium (IV) isopropoxide ($\text{Ti}(\text{OC}_3\text{H}_7)_4$), that will be referred to as TTIP, 97% purity from Aldrich, used as Ti precursor. All chemicals were used as received.

2.2. Preparation procedure

The synthesis method is based on a two-step procedure including an acid in each of both steps: (i) synthesis of the TiO_2 xerogel and (ii) extraction–crystallization of TiO_2 xerogel by treatment with refluxing acid–EtOH mixture. As previously explained, the first step provides materials with highly porous properties but with amorphous titania walls. The extraction–crystallization of the TiO_2 xerogel is carried out in a second step, through a mild acid treatment, which allows a controlled phase transition into the anatase form, while the good textural properties previously produced are maintained.

The detailed synthesis procedure has been performed as follows: TiO_2 nanoparticles were obtained by following a sol–gel route using titanium (IV) isopropoxide as Ti precursor and Pluronic P123 as surfactant [34,37]. In a typical synthesis, Pluronic P123 was first dissolved in a mixture containing isopropanol (purity $\geq 99.8\%$, Sigma–Aldrich) and an aqueous solution of 0.8 M HCl or 0.8 M HI. The resulting solution was slowly stirred for 4 h to favor the organization of the surfactant into micelles. A clear solution was formed and, subsequently, it was added to a solution of titanium isopropoxide in isopropanol with vigorous stirring at 40°C . The sol obtained was kept until a gel appeared at 40°C . The materials so obtained were named $\text{TiO}_2\text{--X}$, where X represents the acid employed in the synthesis of the xerogel (Cl for HCl or I for HI). The chemical molar composition of the gel–precursor solutions for the different samples was as follows:

Samples $\text{TiO}_2\text{--Cl}$: 1TTIP: 34 iPrOH: 0.04HCl: $3\text{H}_2\text{O}$: 0.017P123

Samples $\text{TiO}_2\text{--I}$: 1TTIP: 34 iPrOH: 0.04HI: $3\text{H}_2\text{O}$: 0.017P123

The gels were aged at 40°C so that the total synthesis time was 20 h, and then they were dried under ambient conditions. The TiO_2 xerogel product was extracted–crystallized by reflux treatment (78°C) in mixtures of EtOH–acid (HCl (0.8 M) or HI (0.8 M)) during 24 h and, afterwards, it was centrifuged, washed with ethanol and water, and dried at 60°C .

Subsequently, the materials so obtained were named $\text{TiO}_2\text{--X--Y--Z}$, where X represents the acid employed in the synthesis of the xerogel, (Cl for HCl and I for HI), Y represents the acid employed in the extraction–crystallization (Cl for the HCl–EtOH and I for HI–EtOH) and Z represents the ratio of acid–EtOH (wt%). For comparative purposes, two samples were also prepared using the same synthesis conditions but the surfactant extraction was performed in absence of an acid, using ethanol as solvent (samples $\text{TiO}_2\text{--Cl--0}$ and $\text{TiO}_2\text{--I--0}$).

2.3. Characterization methods

To show the efficiency of the extraction–crystallization step to remove the surfactant from titania thermogravimetric analysis (TGA) was performed on the TiO_2 prepared samples. These analyses were performed from room temperature to 900°C using a STD TA Instruments thermal analyzer at a heating rate of $10^\circ\text{C}/\text{min}$ in a 100 ml/min flow of dried synthetic air.

The porous texture characterization of the samples was obtained from physical adsorption of gases. From N_2 adsorption data at -196°C (Autosorb-6B apparatus from Quantachrome [38]) the specific BET surface area (S_{BET}) and the micropore volume (V_{N_2}) were determined by applying the Brunauer–Emmett–Teller (BET) equation or the Dubinin–Radushkevich equation, respectively. All the samples were outgassed at 250°C under vacuum for 4 h prior to adsorption experiments. The volume of mesopores (2–50 nm, V_{meso}) was estimated as the difference between the volume (expressed as liquid) of N_2 adsorbed at $p/p_0 = 0.9$ and that adsorbed at $p/p_0 = 0.2$ [39]. Total pore volume was determined by the nitrogen adsorption volume at a relative pressure of 0.99.

X-ray powder diffraction was performed to characterize the phase composition and crystal structure of the photocatalysts, using a Siemens D5000 instrument operating at 40 kV/20 mA with Cu $K\alpha$ (1.54\AA) radiation. The scanning velocity was $2^\circ/\text{min}$ and the 2θ scanned ranged from 6° to 80° . The crystallite size was estimated by applying the Scherrer's equation [40] to the main diffraction peak. The synthesized TiO_2 samples were either amorphous or included an important percentage of anatase phase. Rutile or brookite were not detected in any of the samples prepared. In order to determine their crystalline composition, a TiO_2 reference material was prepared submitting several portions of sample $\text{TiO}_2\text{-Cl-Cl-20}$ to different heat-treatment temperatures (from 100 to 400°C) for 5 h. XRD patterns of rutile started to be observed at 300°C , whereas sample heat-treated up to 250°C only showed a well-crystallized anatase structure. Based on such observation, the sample heat-treated up to 250°C was selected and used as the reference material, assuming that is the one having 100% anatase.

Based on the ratio between the intensity of the strongest anatase peak (101) reflection of a given sample and that for the reference sample, the anatase phase was estimated, according to the following equation:

$$R_A\% = \frac{I_{\text{AS}(101\text{ peak})}}{I_{\text{AR}(101\text{ peak})}} \times 100 \quad (1)$$

where R_A is the fraction of anatase phase, and $I_{\text{AS}(101\text{ peak})}$ and $I_{\text{AR}(101\text{ peak})}$ are the intensities of the 101 anatase diffraction peaks of the prepared sample and the reference samples, respectively.

The percentage of amorphous phase, R_{AM} , was then estimated as follows:

$$R_{\text{AM}}\% = 100 - R_A\% \quad (2)$$

In the case of P25, the percentages of amorphous phase, anatase and rutile were obtained from the literature [41].

The UV–vis/DR spectra were analyzed using a UV–vis spectrometer (Jasco V-670) equipped with an integrating sphere accessory and a powder sample holder for diffuse reflectance measurements between 200 nm and 800 nm. The reflectance signal was calibrated with a Spectralon® reference standard (Labsphere SRS-99-010, 99% reflectance). The absorption edge wavelength was estimated from the intercept at zero absorbance of the high slope portion of each individual spectrum. The band gap of the samples can be calculated from the estimated absorption edge wavelength by using the following equation [42]:

$$E_g = \frac{1239.8}{\lambda} \quad (3)$$

where E_g is band gap energy (eV) and λ is wavelength (nm).

For checking the validity of our method, indirect electron transition was supposed and calculation of the band gaps was performed by plotting $(F(R)h\nu)^{0.5}$ vs. $h\nu$, showing the results obtained from the indirect method quite good agreement with those obtained from the method used in the present study.

The morphology of TiO_2 nanoparticles was observed by transmission electron microscopy (TEM) using INCA Energy TEM100 equipment from Oxford Instruments.

2.4. Photocatalytic activities

The photocatalytic performance of the different materials was studied using an experimental system designed in our laboratory. The system consists of a vertical quartz reactor where the photocatalyst bed is placed on quartz wool. The reactor is 50 mm in height, its diameter is 20 mm and the quartz wool support height is around 10 mm. A UV lamp is placed parallel to the quartz reactor, at a distance around 1 cm. The UV lamp radiation peak appears at 365 nm (UV-A). The commercial reference of this lamp is TL 8W/05 FAM, from Philips. Finally, the couple quartz reactor-lamp is surrounded by a cylinder covered with tin foil. A scheme of this system is detailed elsewhere [9].

The weight of photocatalyst used in these experiments was 0.11 g for all the samples. The photocatalysts were used for the oxidation of propene at 100 ppmv in air at room temperature, 25°C . The calibrated gas cylinder was supplied by Carbueros Metálicos, S.A. Different flow rates of the VOC stream, 30 and 60 ml/min (STP), were tested. These flow rates were controlled by mass flow controllers.

The VOC stream passed through the photocatalyst bed and, afterwards, to a mass spectrometer (Balzers, Thermostar GSD 301 01). After suitable calibrations, the mass spectrometer permits to follow the evolution of the concentration of propene in the outlet gas with time.

Before each test, the samples were purged at room temperature with the calibrated cylinder of propene in air that did not contain humidity, until the inlet and outlet concentrations remained constant. Therefore, the tests performed correspond to 0% relative humidity ones. Once samples were purged and propene concentration was stable, the UV light was switched on and the evolution of propene concentration was followed at least for 4 h. Additionally, and to study the stability of the photocatalysts, the two best samples were tested for 40 h.

VOC conversion was calculated using the flowing expression:

$$\text{Propene conversion (\%)} = \frac{C_{\text{initial } C_3H_6} - C_{\text{stationary } C_3H_6}}{C_{\text{initial } C_3H_6}} \times 100 \quad (4)$$

where $C_{\text{initial } C_3H_6}$ is the initial propene concentration, 100 ppmv. $C_{\text{stationary } C_3H_6}$ is the stationary propene concentration in the photocatalyst bed outlet gas when the UV light is switched on.

The amount of CO_2 resulting from propene oxidation was quantified by mass spectroscopy, using a calibrated CO_2 cylinder with a concentration of 300 ppmv.

3. Results and discussion

In the following section, the characterization of the TiO_2 samples and their photocatalytic activity for propene oxidation at low concentration are discussed.

3.1. Porosity characterization of the TiO_2 samples

The N_2 adsorption–desorption isotherms of the different TiO_2 samples prepared are shown in Fig. 1.

Fig. 1a includes samples prepared using HCl in the synthesis of the xerogels and with different extraction–crystallization solutions (pure ethanol, HCl–ethanol or HI–ethanol), while Fig. 1b includes those samples prepared by HI in the synthesis of the xerogels and with different extraction–crystallization solutions (pure ethanol, HCl–ethanol or HI–ethanol).

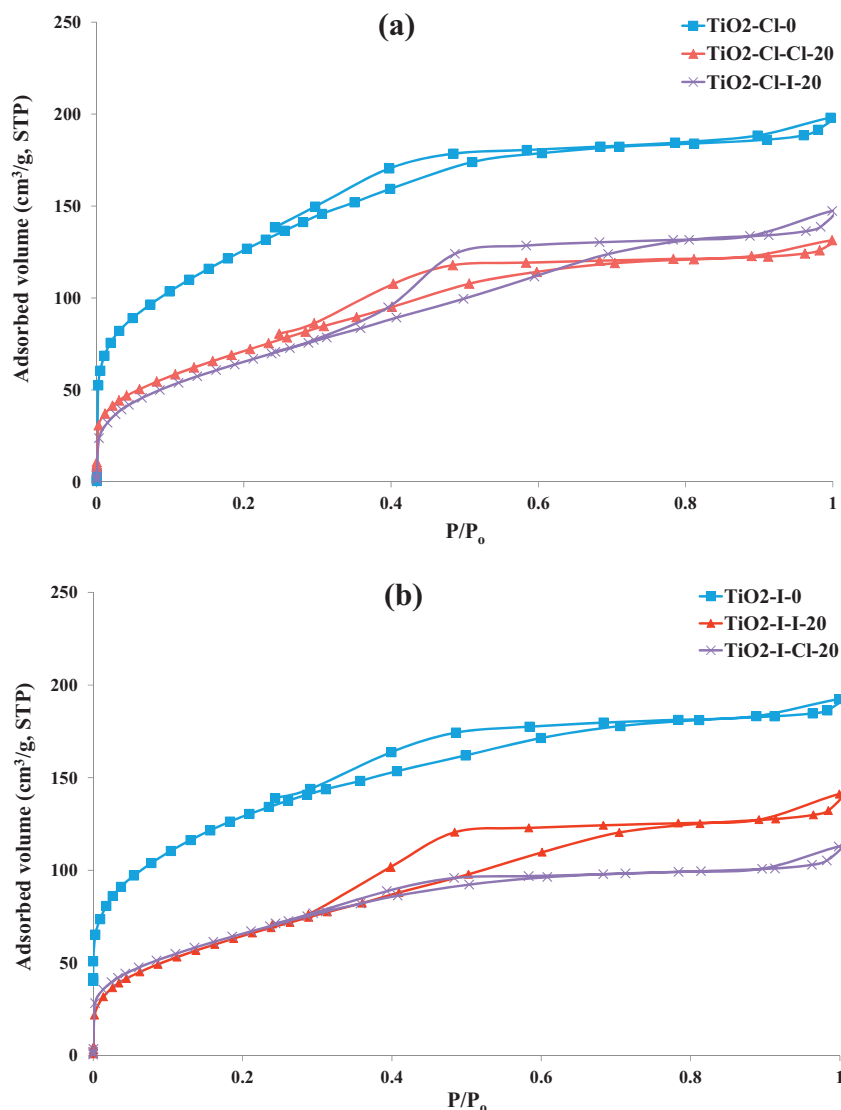


Fig. 1. N₂ adsorption-desorption isotherms at -196°C of the samples synthesized in different conditions with: (a) HCl and (b) HI.

Fig. 1a shows that when using HCl for the preparation of the xerogels, samples are microporous (as noted by adsorption at low relative pressures) and mesoporous (shown by the shape of N₂ adsorption-desorption isotherms, with an important slope at relative pressures over 0.2, and by the presence of hysteresis cycles). Fig. 1b shows similar results when HI is used for the preparation of xerogels instead of HCl. In both Fig. 1a and b, it can be seen that when the extraction-crystallization step is carried out free of acid (i.e., by ethanol) the porous development is much superior to those obtained using acid-EtOH mixtures. These observations point out the negative influence of the presence of an acid in terms of porosity development and its effect in this complex extraction-crystallization step.

The lower porosity developments when an acid is present in the extraction-crystallization step may be related to the fact that the presence of an acid favors some crystal growth, which leads to lower porosity developments, as it will be commented in the next sections.

Another conclusion that can be extracted from Fig. 1a and b is that the shape of the isotherms, in particular the mesopore contribution, is influenced by the acid used during the extraction-crystallization step. Thus, the use of HI-EtOH in this step leads to larger mesoporous contributions.

Table 1 summarizes the main properties of TiO₂ samples prepared. Regarding samples prepared with HCl during the synthesis of the xerogels, it can be observed that surface areas of the materials extracted-crystallized with HCl-ethanol mixtures are similar (compare samples TiO₂-Cl-Cl-20 and TiO₂-Cl-I-20), and much lower than that for the material prepared after the extraction-crystallization step by ethanol (TiO₂-Cl-0), as commented previously from the nitrogen adsorption-desorption isotherms.

Samples derived from xerogels prepared with HI also showed much larger surface area when the materials were prepared by extraction-crystallization with ethanol.

The similar and large surface area of the materials prepared by extraction-crystallization with ethanol (462 and 463 m²/g for TiO₂-Cl-0 and TiO₂-I-0, respectively) could indicate that the extraction of the surfactant is more effective when being performed with ethanol. This point has been analyzed by thermogravimetric analysis over samples TiO₂-Cl-0, TiO₂-I-0, for which extraction-crystallization has been performed in ethanol. Thermogravimetric analysis has proved that when the extraction-crystallization is performed with acids (HCl or HI) or free of acids (only ethanol) effective elimination of the surfactant from the inorganic structure takes place in all cases. This implies

Table 1Physical properties of the TiO₂ nanoparticles extracted by refluxing at different conditions for 24 h (Am: Amorphous, A: Anatase phase).

Sample	S _{BET} (m ² /g)	V _{N₂} (cm ³ /g)	V _{meso} (cm ³ /g)	Total pore volume (cm ³ /g)	Crystalline phase	Crystalline size (nm)
TiO ₂ -Cl-0	462	0.18	0.09	0.31	Am	–
TiO ₂ -Cl-Cl-20	268	0.10	0.09	0.20	A	5
TiO ₂ -Cl-I-20	248	0.09	0.11	0.23	A	6
TiO ₂ -I-0	463	0.19	0.09	0.30	Am	–
TiO ₂ -I-I-20	246	0.09	0.11	0.22	A	6
TiO ₂ -I-Cl-20	246	0.09	0.06	0.17	A	7

Table 2Crystalline properties of TiO₂ determined from XRD patterns. For P25 data have been extracted from [41].

Samples	Amorphous contribution (%)	Anatase (%)	Rutile (%)	Crystalline size (nm)
TiO ₂ -Cl-0	100	–	–	–
TiO ₂ -Cl-Cl-20	18	82	–	5
TiO ₂ -Cl-I-20	9	91	–	6
TiO ₂ -I-0	100	–	–	–
TiO ₂ -I-I-20	10	90	–	6
TiO ₂ -I-Cl-20	23	77	–	7
TiO ₂ -P25	8	78	14	20

that the lower surface of materials extracted in acid–ethanol in comparison to those extracted with ethanol might be due to differences in their crystalline structure, as it will be discussed next.

3.2. X-ray diffraction characterization

The effect of the presence or absence of an acid in the extraction–crystallization step was also analyzed in terms of the crystallinity developed in each material. The crystalline structure of the synthesized TiO₂ samples was analyzed by XRD.

Fig. 2a and b shows XRD patterns of samples prepared using HCl or HI in the synthesis of the xerogels, respectively. Both figures also present the samples for which extraction–crystallization was performed only with ethanol. These two figures show that when the extraction–crystallization is performed in ethanol, the obtained materials are amorphous, in agreement with [34,36], or they have very small crystal sizes so as to be detected by XRD. However, when HCl–EtOH or HI–EtOH are used in the extraction–crystallization, samples are crystalline, no matter the acid used in the preparation of the xerogel. These results agree with the results of porosity, that showed greater areas for the materials extracted–crystallized with ethanol, which also have proved to be the most amorphous ones.

The materials prepared by extraction–crystallization with an acid–ethanol solution contain small anatase crystallites with sizes ranging from 5 to 7 nm, calculated from the width of the main diffraction peak (1 0 1) (JCPDS files no. 21-1272) by applying Scherrer equation [43], see Table 2. It is also important to remark that anatase was detected as the unique crystalline form of titania in the samples treated with acid in the extraction–crystallization. The crystalline properties of TiO₂ nanoparticles, compiled in Table 2, shown that the amorphous percentages are different depending on the nature of the acid used in the extraction–crystallization step; from 9% (TiO₂-Cl-I-20) to 23% (TiO₂-I-Cl-20). Thus, in general the amorphous percentages are a bit larger when HCl is used in the extraction–crystallization step, in comparison to HI.

XRD patterns of samples prepared from xerogels synthesized in HCl or HI (see Fig. 2a and b and Table 2) show that samples for which extraction–crystallization was performed either with HCl–ethanol or HI–ethanol are virtually identical, not only from the porosity point of view (see Table 1), but also because these samples exhibit anatase as the only crystalline phase present, at least detectable by XRD.

In the two series of samples prepared it is observed that the lower crystalline sizes are achieved when the acid used in the extraction–crystallization is the same as that used for the preparation of the xerogel. However, the presence of structural defects, degree of condensation, or other interesting data related with crystallinity cannot be precisely determined by this analytical technique.

3.3. UV–vis analysis of TiO₂ nanoparticles

UV–visible spectra (see Fig. 3) were obtained to evaluate the photoresponse of the TiO₂ materials prepared to the solar spectrum. It can be seen that when hydriodic acid is used in the preparation of the xerogel and, especially when this acid is used in the extraction–crystallization step, UV–visible spectra exhibit an absorption shoulder in the interval between 400 and 700 nm, which is consistent with the spectral range where iodine absorbs [44]. This is especially noticeable in samples TiO₂-I-0, TiO₂-Cl-I-20 and TiO₂-I-I-20, which show a significant broadening in their absorption band compared to those from the TiO₂ samples prepared by HCl acid. The mechanism of the enhanced absorption of the visible light spectrum for TiO₂-I-0 and TiO₂-I-I-20 is not clear. Previous groups have proposed that midgap states and band gap narrowing produce changes in visible–UV absorption [45]. However, this explanation is controversial and lacks sufficient experimental evidence. Recently, Serpone has attributed the enhanced absorption of visible light in TiO₂ treated with hydriodic acid to the formation of oxygen vacancies and to the advent of the Ti³⁺ color centers induced by iodine [46]. Samples TiO₂-I-0, TiO₂-Cl-I-20 and TiO₂-I-I-20 show edge absorption in the interval of 400–650 nm, 400–680 and 400–750 nm, respectively, while samples TiO₂-Cl-0, TiO₂-Cl-Cl-20 and TiO₂-I-Cl-20, prepared by HCl (either during the synthesis of the xerogel or in the extraction–crystallization step) showed an absorption edge at 390 nm, 402 nm and 409 nm, respectively, which is typical for anatase phase. The differences in the absorption edge can be attributed to the combination of acids used, which leads to differences in the prepared semiconductors in terms of their crystalline structure.

As commented above, the absorption measurements of the samples prepared by hydriodic acid show dramatic and strong photoabsorption in the visible light range, from 400 to 700 nm, due to presence of I₂ and/or I₃ as the crystallization temperature is very low to dope TiO₂. The I₂ and/or I₃ comes from the oxidation of I[–], which were not removed during the washing step. The coexistence of I–O–I and I–O–Ti structures may account for the wider range visible light response [47], although the fact that iodine species might be adsorbed on TiO₂, according to previous results [44], cannot either be discarded.

Additionally, Table 3 summarizes the absorption edges (λ) and energy gap values (E_g) of all photocatalysts.

The first absorption edges can be explained in all prepared samples independently of the acid used in terms of charge transition corresponding to the excitation of electrons from the valence band (O 2p) to the conduction band (Ti 3d).

Meanwhile, the second absorption edges of samples TiO₂-I-0, TiO₂-Cl-I-20 and TiO₂-I-I-20 were significantly extended, to

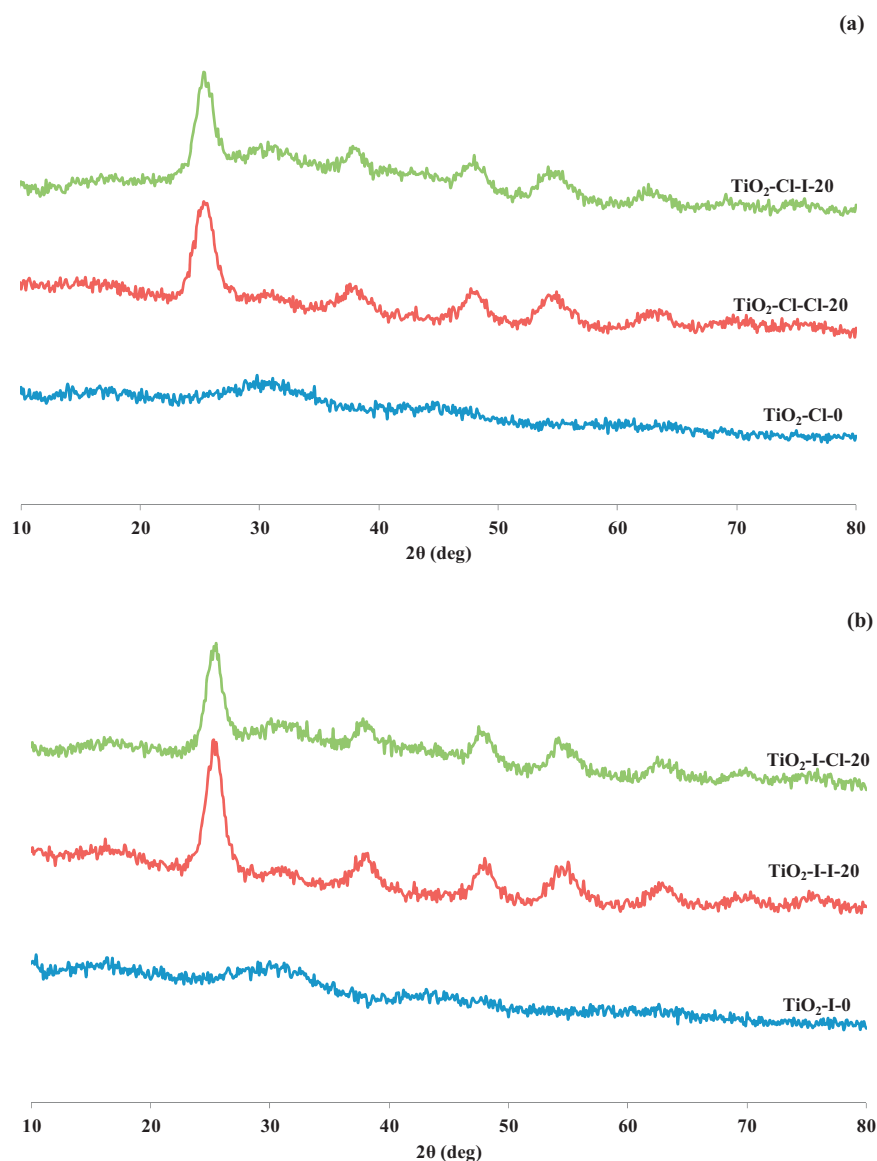


Fig. 2. XRD patterns of the TiO_2 samples extracted by refluxing with ethanol or an acid–ethanol mixture of different compositions for 24 h: (a) samples $\text{TiO}_2\text{-Cl}$ (synthesis of the xerogels using HCl) and (b) samples $\text{TiO}_2\text{-I}$ (synthesis of the xerogels using HI).

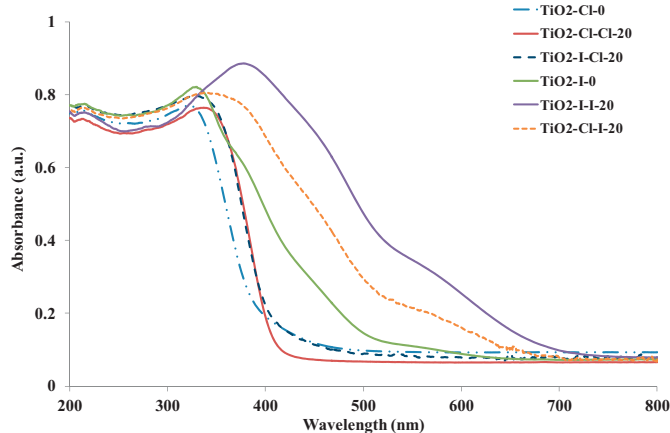


Fig. 3. UV–vis absorption spectra of the TiO_2 prepared samples.

Table 3

Absorption edge wavelengths (λ) and energy gap (E_g) values of all the prepared samples (and $\text{TiO}_2\text{-P25}$ as reference material).

Sample	λ_1 (nm)	E_{g1} (eV)	λ_2 (nm)	E_{g2} (eV)
$\text{TiO}_2\text{-Cl-0}$	390	3.18	–	–
$\text{TiO}_2\text{-Cl-Cl-20}$	402	3.08	–	–
$\text{TiO}_2\text{-Cl-I-20}$	561	2.21	676	1.83
$\text{TiO}_2\text{-I-0}$	519	2.39	640	1.93
$\text{TiO}_2\text{-I-Cl-20}$	409	3.03	–	–
$\text{TiO}_2\text{-I-I-20}$	606	2.04	687	1.80
$\text{TiO}_2\text{-P25}$	409	3.03	–	–

about 700 nm. These samples would greatly improve the absorption of TiO_2 at large wavelengths (as shown in Fig. 4 the absorption in the visible region observed for these samples was much stronger than for those samples prepared using HCl). The band gap for these samples was estimated to be 1.80–2.39 eV.

Hong et al. [48] found that the absorption of iodine-doped TiO_2 samples showed drastic stronger photoabsorption in the range of wavelengths between 400 and 700 nm compared to $\text{TiO}_2\text{-P25}$ and pure TiO_2 . This is in agreement with what it is found in the present

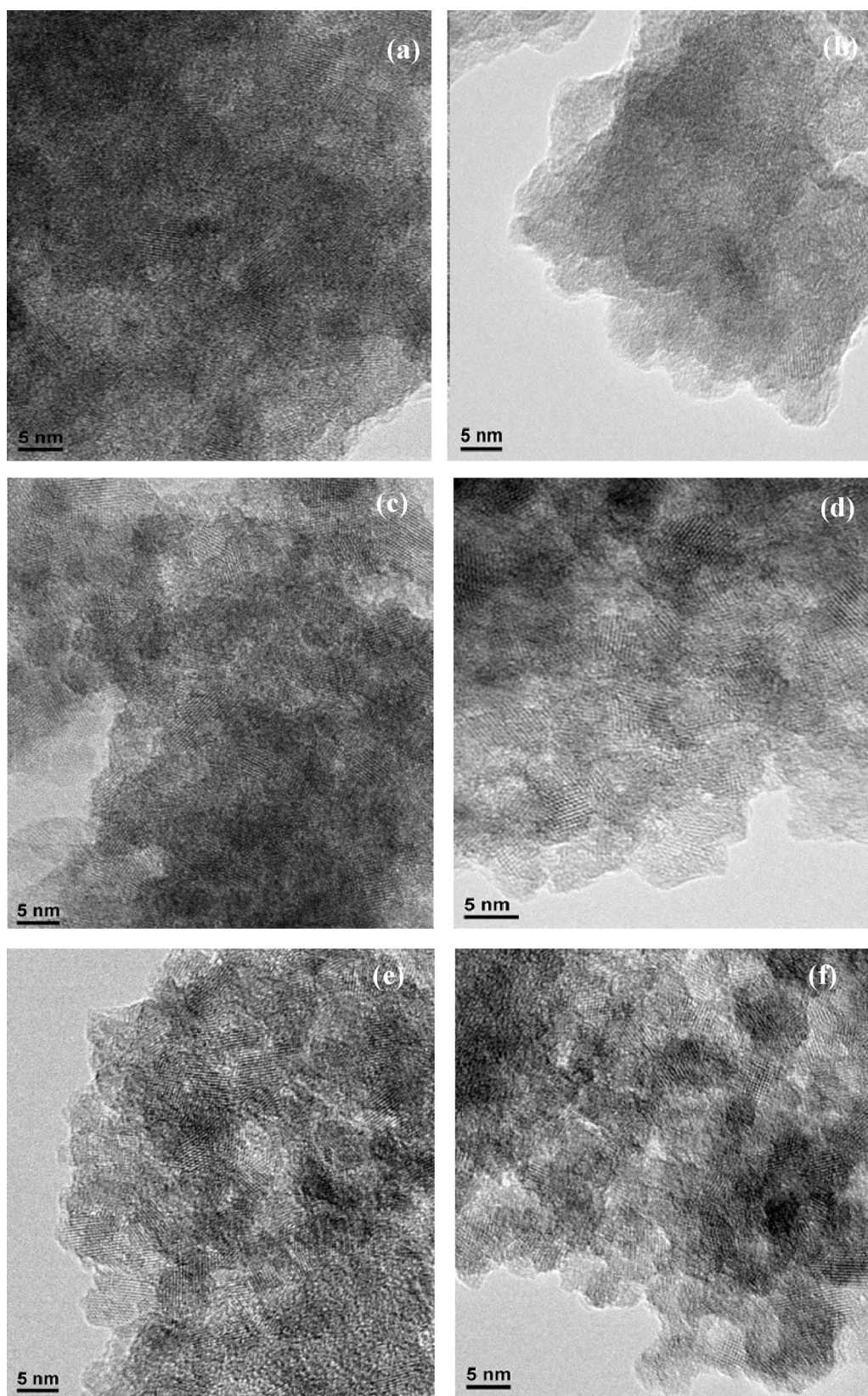


Fig. 4. TEM images of TiO_2 samples: (a) $\text{TiO}_2\text{-Cl-0}$, (b) $\text{TiO}_2\text{-I-0}$, (c) $\text{TiO}_2\text{-Cl-Cl-20}$, (d) $\text{TiO}_2\text{-Cl-I-20}$, (e) $\text{TiO}_2\text{-I-Cl-20}$ and (f) $\text{TiO}_2\text{-I-I-20}$.

study in the case of the $\text{TiO}_2\text{-I-0}$, $\text{TiO}_2\text{-Cl-I-20}$ and $\text{TiO}_2\text{-I-I-20}$ samples: the range of the photoresponse is extended to the visible region with the use of HI acid. The action of iodine reduces the band gap energy by forming doping levels in the band gap of

TiO_2 . When evaluating the absorption change from halogens (Cl and I), we found that the range and intensity become better in visible region with increased molecular weight of elements from chlorine to iodine.

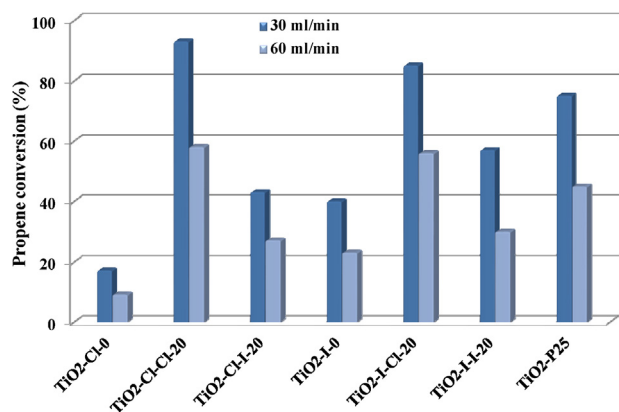


Fig. 5. Propene conversion (at 30 and 60 ml/min) using the different TiO₂ nanoparticles with the 365-nm UV-lamp.

3.4. TEM analysis

Transmission electron microscopy (TEM) was used to characterize the different samples. Fig. 4a and b shows TEM images of samples where the extraction–crystallization has been performed only with EtOH (samples TiO₂-Cl-0 and TiO₂-I-0). The low ordering degree of the TiO₂ structure for these two samples is confirmed. When these images are magnified (images not included), crystal planes that are randomly oriented across the particles can be detected. The presence of these crystalline phases was not observed in the XRD patterns because of the small size of the nuclei [49]. Therefore, it must be remarked that only some parts of the material have some structural ordering when ethanol is the agent used in the extraction–crystallization (samples TiO₂-Cl-0 and TiO₂-I-0), and hence their previously commented amorphous character deduced from XRD.

The TEM images of the TiO₂ nanoparticles prepared after extraction–crystallization step with HCl–EtOH or HI–EtOH are presented in Fig. 4c–f. These images confirm that the acid–EtOH treatment over TiO₂ favors crystallinity in all samples, in comparison to those samples where the extraction–crystallization was performed with ethanol. These results are in agreement with X-ray diffraction patterns, indicating the presence of anatase phase in all samples crystallized with acid–EtOH. The degree of crystallization of the TiO₂ and the size of the nuclei vary depending on the mixture of acid–EtOH used. In general, TEM analysis shows that when HCl is used in the synthesis of the xerogel, the resulting materials are quite crystalline. Let us remark the high crystallinity observed in TiO₂-Cl-Cl-20 (see Fig. 4c).

3.5. Photocatalytic activity of TiO₂ nanoparticles

The use of wavelengths in the range near the solar radiation is of great interest in photocatalysis since it would permit to avoid the use of artificial light for the oxidation of pollutants. In this sense, the present section analyses the use of a UV source with a maximum radiation peak at 365 nm for propene oxidation at low conversion (100 ppmv) in gas phase (air) and at ambient temperature in presence of all the different TiO₂ nanoparticles prepared in this work. The samples prepared have different properties (e.g., surface areas, anatase contents and crystalline sizes and energy band gaps), which will allow to analyze the importance of these variables in their photocatalytic performance. The efficiency of oxidation of propene is shown in Fig. 5.

It is clear that all the prepared materials are active. The samples prepared by ethanol in extraction–crystallization step (TiO₂-Cl-0

and TiO₂-I-0) present the lowest activities toward propene photooxidation with UVA lamp, although they have some activity (being TiO₂-I-0 more active than TiO₂-Cl-0). These results indicate that their similar high surface areas (465 m²/g; Table 1), higher than those for the rest of the prepared materials, and amorphous character (deduced from XRD; Fig. 2) are not beneficial for the oxidation of propene. On the contrary, the two samples prepared using HCl–EtOH in the extraction–crystallization step (TiO₂-Cl-Cl-20 and TiO₂-I-Cl-20) are the most active ones, being both more active than the reference photocatalyst TiO₂-P25. Moreover, the activity of these samples remains constant for at least 40 h, what remarks their stability. This is an interesting result, not only because they possess higher activity than the reference TiO₂-P25 and because of using a 365-nm wavelength source, but also because the results show the importance of using HCl during the extraction–crystallization step, without the need of an additional heat treatment step.

Therefore, results from Fig. 5 remark that the specific surface area of the TiO₂ samples is not governing the photocatalytic oxidation of propene under the experimental conditions analyzed in this study, being the two samples treated by EtOH, that have similar specific surface areas, those presenting the lowest photocatalytic activities, although their specific surface areas are the highest ones. Hence other factors, including crystallinity related ones, might be explaining these results, mainly the anatase content and size, the light absorption efficiency and the electron–hole recombination processes.

Considering data from Tables 2 and 3, it can be observed that neither anatase content nor anatase crystalline size seems to be, in principle, responsible for the good activities of samples TiO₂-Cl-Cl-20 and TiO₂-I-Cl-20 since these samples present lower anatase contents than samples TiO₂-I-I-20 and TiO₂-Cl-I-20 and anatase crystalline size for TiO₂-I-Cl-20 is larger than those for TiO₂-I-I-20 and TiO₂-Cl-I-20. The efficient photoresponse of the TiO₂ samples prepared with HCl–EtOH in the extraction–crystallization step, TiO₂-Cl-Cl-20 and TiO₂-I-Cl-20, in comparison to the other samples, can be attributed to the fact that the wavelength of the lamp used (UVA, 365 nm) is appropriate for the electron excitation to the conduction band. Thus, it must be recalled that the absorption edge wavelength for these two samples is 402 and 409 nm, respectively, (see Table 3) and the more similar the wavelength of the radiation used and the energy band gap value, the more efficient the electron promotion [50].

The fact that TiO₂-Cl-Cl-20 and TiO₂-I-Cl-20 present larger amorphous contributions, in the range of 20%, in comparison to TiO₂-I-I-20 and TiO₂-Cl-I-20, with amorphous contributions around 10%, could also be an advantage for diminishing the electron–hole recombination processes.

Despite the advantages commented in the literature regarding the fact that the use of hydriodic acid improves the photoresponse of the prepared samples in the visible light region [51–53], in the case of the samples extracted–crystallized with hydriodic acid, lower propene conversions are achieved than in the previous set of samples. Let us remember that all the samples extracted–crystallized with mixtures acid–ethanol present similar porosities and anatase crystalline phase, with some differences from the point of view of crystalline size and amorphous phase composition already mentioned. However, it must be remarked that the first absorption edge wavelengths for TiO₂-Cl-I-20 and TiO₂-I-I-20 are 561 and 606 nm, respectively, in contrast to 402 and 409 nm in TiO₂-Cl-Cl-20 and TiO₂-I-Cl-20, respectively. This means that the electron–hole pairs generation process is more efficient for TiO₂-Cl-Cl-20 and TiO₂-I-Cl-20, and hence these samples show higher propene conversions.

4. Conclusions

Nanostructured TiO₂ photocatalysts have been synthesized by a new sol–gel synthesis route which consists of the treatment of TiO₂ xerogels with two types of acid–ethanol mixtures in two different steps, synthesis and extraction–crystallization at low temperature, 78 °C, and using Pluronic P123 as template.

The materials prepared by the use of HCl and HI solutions present surface areas ranging from 250 to 460 m²/g, with an important contribution of micro and mesoporosity, and different degrees of crystallinity depending on the experimental conditions used. When using pure ethanol in extraction–crystallization large surface area amorphous TiO₂ is obtained, whereas when using acid–ethanol mixtures very small size anatase crystals, ranging from 5 to 7 nm, are obtained.

The prepared samples exhibit significant photocatalytic activity for propene oxidation at low concentration (100 ppmv) in gas phase using UVA lamp. In particular, the use of HCl–EtOH mixture for the extraction–crystallization step provides the best photocatalytic properties, superior than the reference commercial P25 from Evonik (previously known as Degussa), due to the crystallinities and small anatase phase sizes and, especially, because of the similarity between radiation used, 365 nm, and the absorption edge wavelengths of these materials, 402–409 nm, confirmed by UV–vis spectra analysis, which provide very good photocatalytic performance.

Acknowledgements

M. Ouzzine thanks MAEC-AECID for a predoctoral fellowship. J.A. Maciá-Agulló acknowledges the assistance of the Spanish MCyT for their award of a Postdoctoral Juan de la Cierva contract. The authors thank Generalitat Valenciana (GVPRE/2008/004, PROMETEO/2009/047), FEDER, MINECO (MAT2010-15273) and Office of the Vice President for Research, Development and Innovation of University of Alicante (UAUSTI10-08) for financial support.

References

- [1] A. Fujishima, T.N. Rao, D.A. Tryk, *Journal of Photochemistry and Photobiology C: Photochemistry Reviews* 1 (2000) 1–21.
- [2] J.G. Yu, J.C. Yu, M.K.-P. Leung, W.K. Ho, B. Cheng, X.J. Zhao, J.C. Zhao, *Journal of Catalysis* 217 (2003) 69–78.
- [3] M. Anpo, M. Takeuchi, *Journal of Catalysis* 216 (2003) 505–516.
- [4] F.W. Lurmann, H.H. Main, Analysis of the ambient VOC data collected in the Southern California Air Quality Study, Report prepared for the California Air Resources Board, Sacramento, STI-99120-1161-FR, Contract no. A823-130, CA by Sonoma Technology, Inc, Santa Rosa, CA, February 1992.
- [5] C.F. Murphy, D.T. Allen, *Atmospheric Environment* 39 (2005) 3785–3798.
- [6] F. Mühlberger, T. Streibel, J. Wieser, A. Ulrich, R. Zimmermann, *Analytic Chemistry* 77 (2005) 7408–7414.
- [7] M.A. Lillo-Ródenas, N. Bouazza, A. Berenguer-Murcia, J.J. Linares-Salinas, P. Soto, A. Linares-Solano, *Applied Catalysis B: Environmental* 71 (2007) 298–309.
- [8] N. Bouazza, M.A. Lillo-Ródenas, A. Linares-Solano, *Applied Catalysis B: Environmental* 77 (2008) 284–293.
- [9] N. Bouazza, M.A. Lillo-Ródenas, A. Linares-Solano, *Applied Catalysis B: Environmental* 84 (2008) 601–609.
- [10] N. Bouazza, M. Ouzzine, M.A. Lillo-Ródenas, A. Linares-Solano, *Applied Catalysis B: Environmental* 92 (2009) 377–383.
- [11] M. Ouzzine, M.A. Lillo-Ródenas, A. Linares-Solano, *Applied Catalysis B: Environmental* 127 (2012) 291–299.
- [12] M. Ouzzine, M.A. Lillo-Ródenas, A. Linares-Solano, *Applied Catalysis B: Environmental* 134 (2013) 333–343.
- [13] A.L. Linsebigler, G. Lu, J.T. Yates, *Chemical Reviews* 95 (1995) 735–758.
- [14] M. Schiavello, *Heterogeneous Photocatalysis*, vol. 3, Wiley, New York, 1997.
- [15] C.B. Almquist, P. Biswas, *Journal of Catalysis* 212 (2002) 145–156.
- [16] J. Ovenstone, *Journal of Materials Science* 36 (2001) 1325–1329.
- [17] Z. Zhang, C.C. Wang, R. Zakaria, J.Y. Ying, *Journal of Physical Chemistry B* 102 (1998) 10871–10878.
- [18] C.-C. Wang, Z. Zhang, J.Y. Ying, *Nanostructured Materials* 9 (1997) 583–593.
- [19] M. Grela, A.J. Colussi, *Journal of Physical Chemistry B* 100 (1996) 18214–18221.
- [20] N. Xu, Z. Shi, Y. Fan, J. Dong, J. Shi, M.Z.-C. Hu, *Industrial & Engineering Chemistry Research* 38 (1999) 373–383.
- [21] A.J. Maira, K.L. Yeung, C.Y. Lee, P.L. Yue, C.K. Chan, *Journal of Catalysis* 192 (2000) 185–196.
- [22] S. Sahni, S.B. Reddy, B.S. Murty, *Materials Science and Engineering: A* 452/453 (2007) 758–762.
- [23] B. Li, X. Wang, M. Yan, L. Li, *Materials Chemistry and Physics* 78 (2002) 184–188.
- [24] Y.V. Kolen'ko, B.R. Churagulov, M. Kunst, L. Mazerolles, C. Colbeau-justin, *Applied Catalysis B: Environmental* 54 (2004) 51–58.
- [25] W. Zhou, Q. Cao, S. Tang, *Powder Technology* 168 (2006) 32–36.
- [26] J.C. Yu, J.G. Yu, W.K. Ho, L.Z. Zhang, *Chemical Communications* 19 (2001) 1942–1943.
- [27] H. Liu, W. Yang, Y. Ma, Y. Cao, J. Yao, *New Journal of Chemistry* 26 (2002) 975–977.
- [28] J.G. Yu, J.C. Yu, *Chinese Journal of Chemistry* 21 (2003) 994–997.
- [29] J.G. Yu, J.C. Yu, W.K. Ho, Z.T. Jiang, *New Journal of Chemistry* 26 (2002) 607–613.
- [30] C.-C. Wang, Y. Ying, *Chemistry of Materials* 11 (1999) 3113–3120.
- [31] G.J.A.A. Soler-Illia, D. Grosso, E.L. Crepaldi, F. Cagnol, C. Sánchez, *Materials Research Society Symposia Proceedings* 726 (2002) 243–248.
- [32] A.R. Liu, S.M. Wang, Y.R. Zhao, Z. Zheng, *Materials Chemistry and Physics* 99 (2006) 131–134.
- [33] Y.-Q. Wang, S.-G. Chen, X.-H. Tang, O. Palchik, A. Zaban, Y. Koltypin, A. Gedanken, *Journal of Materials Chemistry* 11 (2001) 521–526.
- [34] D.P. Serrano, G. Calleja, R. Sanz, P. Pizarro, *Chemical Communications* 10 (2004) 1000–1001.
- [35] Y. Ao, J. Xu, D. Fu, *Applied Surface Science* 256 (2009) 239–245.
- [36] D.P. Serrano, G. Calleja, R. Sanz, P. Pizarro, *Journal of Materials Chemistry* 17 (2007) 1178–1187.
- [37] G. Calleja, D.P. Serrano, R. Sanz, P. Pizarro, A. Garcia, *Industrial & Engineering Chemistry Research* 43 (2004) 2485–2492.
- [38] J. Rouquerol, F. Rouquerol, K.S.W. Sing, *Adsorption by Powders and Porous Solids: Principles, Methodology and Applications*, Academic Press, San Diego, 1999.
- [39] F. Rodríguez-Reinos, A. Linares-Solano, Microporous structure of activated carbons as revealed by adsorption methods, in: P.A. Thrower (Ed.), *Chemistry and Physics of Carbon*, vol. 21, Marcel Dekker, New York, 1988, pp. 1–146.
- [40] H. Zhang, J.F. Banfield, *Journal of Physical Chemistry B* 104 (2000) 3481–3487.
- [41] B. Ohtani, O.O. Prieto-Mahaney, D. Li, R. Abe, *Journal of Photochemistry and Photobiology A: Chemistry* 216 (2010) 179–182.
- [42] A.R. Gandhe, J.B. Fernandes, *Journal of Solid State Chemistry* 178 (2005) 2953–2957.
- [43] H. Klug, L. Alexander, *X-ray Diffraction Procedures*, second ed., John Wiley & Sons, New York, 1962.
- [44] P.K. Stoimenov, V. Zaikovski, K.J. Klabunde, *Journal of the American Chemical Society* 125 (2003) 12907–12913.
- [45] R. Asahi, T. Morikawa, T. Ohwaki, K. Aoki, Y. Taga, *Science* 293 (2001) 269–271.
- [46] N. Serpone, *Journal of Physical Chemistry B* 110 (2006) 24287–24293.
- [47] G. Liu, C.H. Sun, X.X. Yan, L. Cheng, Z.G. Chen, X.W. Wang, L.Z. Wang, S.C. Smith, G.Q. Lu, H.M. Cheng, *Journal of Materials Chemistry* 19 (2009) 2822–2829.
- [48] X.T. Hong, Z.P. Wang, W.M. Cai, F. Lu, J. Zhang, Y.Z. Yang, N. Ma, Y.J. Liu, *Chemistry of Materials* 17 (2005) 1548–1552.
- [49] B.L. Bischoff, M.A. Anderson, *Chemistry of Materials* 7 (1997) 1772–1778.
- [50] J. Zhao, X. Yang, *Building and Environment* 38 (2003) 645–654.
- [51] Y. Ma, J.-W. Fu, X. Tao, X. Li, J.-F. Chen, *Applied Surface Science* 257 (2011) 5046–5051.
- [52] V. Štengl, T.M. Grygar, *International Journal of Photoenergy* (2011), <http://dx.doi.org/10.1155/2011/685935>.
- [53] X. Hong, Z. Luo, J.D. Batteas, *Journal of Solid State Chemistry* 184 (2011) 2247–2249.